Journal of Molecular Graphics and Modelling 42 (2013) 39–49

Contents lists available at SciVerse ScienceDirect

Journal of Molecular Graphics and Modelling

journal homepage: www.elsevier.com/locate/JMGM

Pharmacophore modeling, homology modeling, and *in silico* screening reveal mammalian target of rapamycin inhibitory activities for sotalol, glyburide, metipranolol, sulfamethizole, glipizide, and pioglitazone

Mohammad A. Khanfar[a], Majed M. AbuKhader[b], Saja Alqtaishat[a], Mutasem O. Taha[a,*]

[a] Drug Discovery Unit, Department of Pharmaceutical Sciences, Faculty of Pharmacy, University of Jordan, Amman 11942, Jordan
[b] Department of Pharmacy, Oman Medical College, Muscat, Oman

ARTICLE INFO

Article history:
Accepted 24 February 2013
Available online 13 March 2013

Keywords:
mTOR
HipHop
Pharmacophore
Virtual Screening
Homology model
ROC

ABSTRACT

Mammalian target of rapamycin (mTOR) is a serine/threonine kinase and member of the PI3K-related kinase (PIKK) family. It plays a central role in integrating signals from metabolism, energy homeostasis, cell cycle, and stress response. Aberrant PI3K/mTOR activation is commonly observed in diseases such as cancer, diabetes and Alzheimer's disease. Accordingly, we developed common feature binding hypotheses for a set of 6 potent mTOR antagonists. The generated models were validated using receiver operating characteristic (ROC) curve analyses. To gain better insight into ligand–mTOR interactions, a homology model for the kinase domain of mTOR was built using the crystallographic structure of PI3Kγ as template. The optimal pharmacophore model was further improved based on detailed docking studies of potent training compound in the homology model. The modified binding model was employed as 3D search query to screen our in-house-built database of established drugs. Subsequent in vitro screening of captured hits showed that six of them have submicromolar to low micromolar bioactivities, namely, glyburide, metipranolol, sulfamethizole, glipizide, pioglitazone, and sotalol.

1. Introduction

Mammalian target of rapamycin (mTOR) is a serine/threonine kinase and member of the PI3K-related kinase (PIKK) family [1]. It plays a central role in integrating signals from metabolism, energy homeostasis, the cell cycle, and the stress response [1,2]. Aberrant PI3K/mTOR activation is commonly observed in cancers [3] and can result from amplification of, or activating mutations in, genes encoding the upstream RTKs, components of PI3K, or effector kinases [4]. mTOR plays a key role in supporting tumor cell survival and proliferation under metabolic stress conditions by affecting the equilibrium between gluconeogenesis and glycolysis in response to the cell energy supply and regulation of glucose transporters [5]. mTOR drives cancer growth by activating the lipid and protein biosynthesis needed for robust tumor expansion. It is reported that mTOR regulates actin reorganization and cancer cell proliferation [6]. In hypoxic cancer tissue, mTOR participates in HIF-1α activation to support cell survival [7]. Inhibition of mTOR leads to mitotic cells arresting in G1, possibly through down-regulation of Cyclin D1 translation, which may eventually result in cell death through apoptosis [8]. Therefore, mTOR is a validated target for cancer treatment [9]. In addition to cancer, mTOR contributes in the progression of Alzheimer's disease (AD). It is hyperactivated in the brains of AD patients and it seems to be responsible for the development of amyloid beta (Aβ) and tau proteins, which aggregate and form two hallmarks of the disease, Aβ plaques and neurofibrillary tangles, respectively [10,11]. Over-stimulation of the mTOR pathway by excess food consumption may be a crucial factor underlying the diabetes [12]. mTOR hyperactivation during hyperfeeding leads to insulin desensitization. This results in dampened Akt activation, which translates into reduced glucose uptake and glycogen synthesis in liver and muscle, and increased gluconeogenesis and glucose release by the liver. Collectively, these effects lead to a worsening of the hyperglycaemia and hyperinsulinaemia [12].

The great recent interest in developing new mTOR inhibitors as potential agents for treatment of cancer, AD, and diabetes [1–12], combined with the lack of crystallographic structure for mTOR kinase domain, prompted recent efforts to develop corresponding ligand-based QSAR and pharmacophore models [13–15], albeit without subsequent implementation in design or discovery (i.e., via *in silico* screening) of new mTOR inhibitors.

Accordingly, we were prompted to develop several pharmacophore models for 6 most potent mTOR inhibitors. One of the developed pharmacophores models illustrated excellent receiver-operating characteristic (ROC) curve analysis. However, to further understand the optimal pharmacophore model within the context of ligand–receptor binding interactions into the kinase

* Corresponding author. Tel.: +962 65355000x23305; fax: +962 65339649.
E-mail address: mutasem@ju.edu.jo (M.O. Taha).

1093-3263/$ – see front matter © 2013 Elsevier Inc. All rights reserved.
http://dx.doi.org/10.1016/j.jmgm.2013.02.009

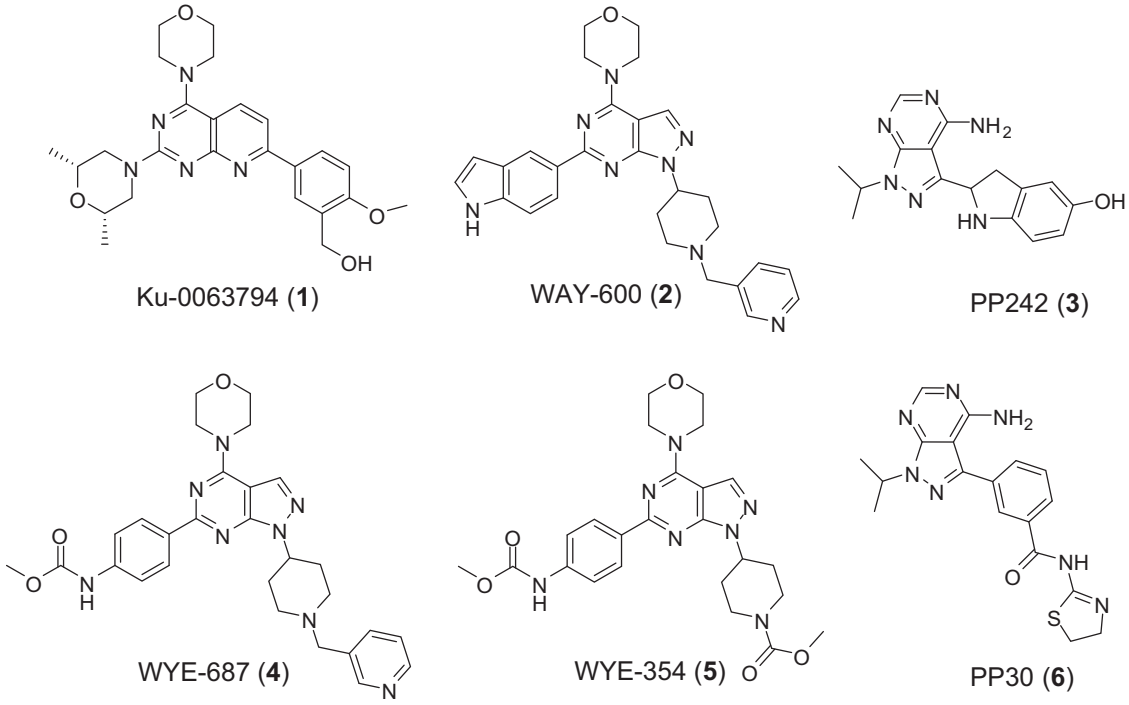

Fig. 1. The structures of the training compounds.

binding site of mTOR, we docked the most potent training compound (**5**, Fig. 1) into a homology model we constructed for mTOR kinase domain. Interestingly, the binding features of the optimal pharmacophore model closely correlated with binding interactions unveiled by docking. Nevertheless, we slightly modified the optimal pharmacophore based on information harnessed from the docking/homology modeling study.

Finally, we implemented the resulting pharmacophore model as 3D search query to screen our *in-house*-built database of established drug molecules, to identify mTOR inhibitory hits from drug space. Six drug hits illustrated submicromolar to low micromolar anti-mTOR IC_{50} values. Such hits are expected to be excellent leads for subsequent optimization because they have established toxicological and SAR profiles.

2. Methods

2.1. Pharmacophore modeling

2.1.1. Conformational analysis

The conformational space of each inhibitor (**1**–**6**) was explored adopting the "CAESAR" option within CATALYST [16–18]. Detailed conformational analysis is provided in the supplementary material (section SM-1).

2.1.2. Common feature pharmacophore model generation

We employed the HipHop module [16,19,20] of CATALYST software to construct plausible binding hypotheses for mTOR antagonists. Detailed experimental and theoretical explanations are provided in the supplementary material (section SM-2).

2.2. Homology modeling

2.2.1. Software and protein sequence

Homology modeling was performed through the web-based port of the Automated Comparative Protein Modeling Server (SWISSMODEL, http://swissmodel.expasy.org//SWISS-MODEL.html) [21]. The resulting homology structure was assessed using the protein structure verification WHAT-CHECK [22,23] module of the WHATIF on-line server (http://swift.cmbi.ru.nl/servers/html/index.html). The model was visualized on a personal computer using the DeepView-pdb viewer shareware (version 4.1) provided on-line via SWISSMODEL web-site (http://spdbv.vital-it.ch/). All sequence data were obtained from the National Center for Biotechnology Information (NCBI, http://www.ncbi.nlm.nih.gov). The accession numbers for mTOR and template structure PI3Kγ are P42345 and O02697, respectively.

2.2.2. Homology modeling steps

SWISS-MODEL [21,24,25] was applied for homology modeling of mTOR kinase domain applying PI3Kγ protein bound to wortmannin (PDB ID = 1E7U) [26] as a template. Several sequential alignments of 1E7U and mTOR were performed by means of ClustalW via four scoring matrices (Blosum, Gonnet, Identity and Pam) and different gap penalty combinations, as in Table 3. Detailed experimental homology modeling steps are provided in the supplementary material (see section SM-3).

2.2.3. Analysis of the homology models

The resulting homology structures were evaluated employing the WHAT-CHECK module of the WHATIF on-line server. Table 4 shows the summary outputs of WHAT-CHECK calculated for the generated homology structures and their consensus votes. See SM-4 in the supplementary material for more details.

2.3. Docking settings

Docking experiments were conducted employing LigandFit docking engine [27]. In the current docking experiments, the binding site was generated from the "Find sites from receptor cavities" option in DiscoveryStudio2.5 as defined in literature [28]. High-ranking docked conformers/poses were scored using six scoring functions: Jain [29], LigScore1, LigScore2 [27,30], PLP1 [31], PLP2 [32], and PMF [33]. Implemented docking configurations and their

Table 1
The training list used for pharmacophore modeling of mTOR inhibitors.

Compounds	Bioactivities (IC_{50}, nM)	Principal value	MaxOmitFeat	Best fit values against Hypo1
1	10	2	0	6.00
2	9	2	0	4.56
3	8	2	0	1.13
4	7	2	0	3.67
5	5	2	0	3.06
6	80	1	1	1.08

theoretical explanations are shown in details in section (SM-5) in the supplementary material.

2.4. Bioassay of captured hits

Tested hits, i.e., sotalol, glyburide, metipranolol, sulfamethizole, glipizide, pioglitazone, esmolol, and sulfamethoxazole, were purchased as analytical standards from Sigma–Aldrich, USA. The mTOR inhibitory activities of captured hits were assessed using Z′-LYTE™ biochemical assay from Invitrogen using PF-04691502 as standard mTOR inhibitor. Briefly, recombinant mTOR was purchased from Invitrogen (Carlsbad, CA). The mTOR kinase assays were carried out with the Invitrogen Z′-LYTE™ Kinase Assay kit. The assay was optimized for use with mTOR as described in Invitrogen protocol. The mTOR concentration was optimized to obtain the desired percent phosphorylation with an acceptable *Z′*-factor value, which indicates the quality of an assay; *Z′*-factor values of 0.5 or greater classify an assay as excellent. A *Z′*-factor value of 0.74 was obtained at final kinase and ATP concentrations of 14 nM and 100 μM, respectively. Tested concentrations ranged from 10 nM to 10 μM distributed log-linearly across the concentration range, and at least two data points from each concentration were collected. The IC_{50} value for each experiment was obtained using nonlinear regression of the log(concentration) versus percent inhibition values (GraphPad Prism 5.0). The assay conditions were validated by running positive (PF-04691502) and negative (provided in Z′-LYTE™ Kinase Assay kit) controls.

3. Results and discussion

3.1. Pharmacophore modeling

We employed the HipHop module of CATALYST software to build reasonable binding hypotheses. In this project, we employed six highly active standard mTOR inhibitors as training set for pharmacophore modeling (Fig. 1, Table 1) [34–37]. A conformational database for each of the training compounds was generated using the 'CAESAR' option.

HipHop identifies 3D spatial arrangements of chemical features that are common to active molecules in a training set. Principal and MaxOmitFeat parameters define how many molecules must map completely or partially to the hypothesis. After several trials; it was decided to configure HipHop as follows. Inhibitors **1**–**5** (Fig. 1), which have potent inhibitory actions against mTOR were assigned a principal value of 2 (Table 1) to ensure that all of the chemical features in the compound will be considered in building the pharmacophore space (Catalyst User Guide, Accelrys Software Inc.). On the other hand, compound **6** (Fig. 1), which is 8–16 times less active than inhibitors **1**–**5**, was assigned a principal value of 1 (Table 1) to ensure that it will be mapped at least once by each generated hypothesis. However, compound **6** was allowed to miss one feature in any generated model by assigning it a MaxOmitFeat parameter of one (Table 1), while the remaining compounds were assigned a MaxOmitFeat of 0 to instruct HipHop that they should not miss any feature during pharmacophore modeling (Table 1).

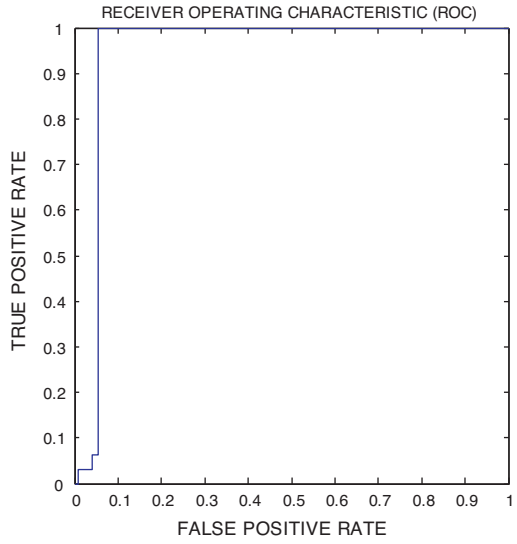

Fig. 2. Receiver operating characteristic (ROC) curve of Hypo1.

HipHop was asked to explore up to 6-featured pharmacophoric space of the following possible features: hydrogen bond donors and acceptors (HBDs and HBAs), hydrophobic (Hbic) and aromatic (RingArom). Moreover, the number of features of any particular type was allowed to vary from 3 to 4 for HBA, 0 to 1 for HBD, 0 to 1 for RingArom, and 0 to 1 for Hbic. Finally, HipHop was constructed to permit a minimal inter-feature distance of 1 Å to build the hypothesis. It was found that higher-feature pharmacophores were too restrictive and of limited coverage, i.e., limited number of hits was captured upon use as 3D search query. On the other hand, lower-featured pharmacophores are non-selective and tend to capture large number of hits.

Ultimately, 10 optimal pharmacophoric hypotheses were created. The generated hypotheses share the same number of features; 4 HBAs, 1 hydrophobic, and 1 aromatic feature, but with different 3D spatial arrangements (Table 2).

To validate the resulting models, we subjected our pharmacophores to ROC analysis to assess their abilities to selectively capture diverse mTOR inhibitors from a large list of decoys. The decoy list was prepared as described by Verdonk and co-workers [38,39] and described in the supplementary material (see section SM-6). Active testing compounds were defined as those possessing mTOR affinities (IC_{50} values) ranging from 0.1 nM to 61 nM. The testing set included 32 active compounds (retrieved from literature [40–43] and their structures are depicted in Fig. A in the supplementary material) and 1322 ZINC compounds. The ROC testing set (1354 compounds) was screened by each pharmacophore for ROC analysis employing the "Best rigid search" option implemented in CATALYST. The validity of a particular pharmacophore is indicated by the area under the curve (AUC) of the corresponding ROC curve, as well as accuracy, specificity, true positive rate and false negative rate of the pharmacophore [38,39]. To rank the pharmacophores based on ROC properties, we employed a consensus voting approach in which each individual ROC property casts a vote if the corresponding value of the considered pharmacophore falls within the highest 50% range of that property across all pharmacophores. The consensus vote is the total number of votes received. Table 2 summarizes different pharmacophoric success criteria including the number of votes given for each pharmacophores. Clearly from Table 2, Hypo1 showed excellent overall properties. Fig. 2 shows the ROC curve of Hypo1. Fig. 3 shows Hypo1

Table 2
HipHop-generated hypotheses and their ROC analysis results.

Hypotheses	Hypothesis rank[a]	AUC[b]	FNR[c]	TPR[d]	SPC[e]	ACC[f]	Consensus voting[g]
Hypo1	96.12	0.948	0.0021	0.0625	0.998	0.968	5
Hypo2	95.47	0.939	0.0031	0.0938	0.997	0.968	4
Hypo3	95.07	0.936	0.0010	0.0313	0.999	0.968	3
Hypo4	94.39	0.912	0.0031	0.0938	0.997	0.968	3
Hypo5	93.40	0.926	0.0010	0.0313	0.999	0.968	3
Hypo6	93.21	0.935	0.0010	0.0313	0.999	0.968	3
Hypo7	92.79	0.859	0.0031	0.0938	0.997	0.968	3
Hypo8	92.66	0.925	0.0011	0.0625	0.998	0.968	3
Hypo9	92.24	0.838	0.0073	0.0206	0.993	0.966	1
Hypo10	92.21	0.886	0.0021	0.0625	0.998	0.968	4

[a] This ranking is as provided in the log file of the HipHop automatic run. The ranking is a measure of how well the active training molecules map onto the proposed pharmacophores, as well as the rarity of the pharmacophore models
[b] AUC: area under the curve.
[c] FNR: overall false negative rate.
[d] TPR: overall true positive rate.
[e] SPC: overall specificity.
[f] ACC: overall accuracy.
[g] A consensus voting approach in which each individual ROC property casts a vote if the value of the considered binding model falls in the highest-ranking 50% of the range of values obtained for the particular ROC property across different binding models. The consensus vote is the total number of votes received.

and how it maps **5**, as well as other training compounds. The ROC curves of all models are provided in the supplementary material.

3.2. Homology modeling of mTOR kinase domain and docking experiment

To gain better insights into the ligand–receptor binding interactions denoted by binding features of optimal pharmacophore (Hypo1), it was decided to build an appropriate homology model for mTOR kinase domain followed by docking the most potent training compound (**5**, Fig. 1, Table 1) into the homologous binding pocket. Comparison between the optimal pharmacophore and corresponding docking-based ligand–mTOR interactions should allow better assessment of the significance individual binding features proposed by Hypo1.

Homology modeling was performed employing SWISS-MODEL server [21] and based on several ClustalW [24] pair-wise alignments. The kinase domain of mTOR was aligned against the crystallographic structure of closely related PI3Kγ (PDB ID = 1E7U) bound to wortmannin [26]. This particular protein structure was selected as template for modeling mTOR because it has the best crystallographic resolution among PI3Kγ complexes in the protein data bank (2.0 Å), and the fact that it is complexed with a potent known mTOR inhibitor (i.e., wortmannin). Three homology models were generated, i.e., A, B, and C (see Table 2). The models were evaluated by their WHATIF Quality Control values [44]. WHATIF generates a summary report of the overall quality of the protein structure as compared with current reliable protein structures presented in the form of RMS *Z*-scores [44]. Table 4 shows the summary output of WHATIF criteria for the generated homology structures (A, B, and C).

To rank the resulting homology structures, we employed a consensus voting approach in which each individual WHATIF property casts a vote if the corresponding value of the considered structure falls within the highest 50% range obtained for that property across the different homology models. The consensus vote is the total number of votes received. Table 4 shows the number of votes given for each homology structure.

Models A received the highest number of votes (9), while remaining models, i.e., B and C, scored significantly lower (6 votes each) suggesting their general poorer qualities. Therefore, it was decided to select homology model A for subsequent docking/scoring modeling.

Fig. 4 shows details of sequence similarities and identities among homology model A and the corresponding PI3Kγ template. Clearly from the figure, model A shows 20.1% and 23.6% sequence identity and similarity, respectively, with template structure. Interestingly, 7 out of 9 binding site amino acids in homology model A are identical with their counterparts in PI3Kγ template, which enhances confidence in the accuracy of the homologous binding site (Fig. 4). Previous reports have strongly suggested that PI3Kγ and mTOR have almost identical binding sites [28,45]. Fig. 5A shows 3D presentations of homology model A superimposed over PI3Kγ template.

With the availability of plausible binding site structure for mTOR we proceeded to docking experiment. Molecular docking was performed employing LigandFit docking engine. The resulting docking solutions were scored by six different scoring functions: Jain [29], LigScore1, LigScore2 [27,30], PLP1 [31], PLP2 [32], and PMF [33]. The best docked pose of compound **5** (WYE-354) was selected based on consensus among all 6 scoring functions. Fig. 3D and E shows the docked pose of **5** into the putative binding pocket of mTOR.

Interestingly, the docked pose of **5** within mTOR homology structure seems to starkly contrast with poses of related co-crystallized ligands within PI3Kγ. Fig. 5 compares the docked pose of **5** with co-crystallized complexes of wortmannin (PDB code 1E7U) and GDC0941 (PDB code 3DBS) within PI3Kγ binding pocket. Both compounds are dual mTOR and PI3Kγ inhibitors.

Clearly from Fig. 5A–C, wortmannin and GDC0941 share two common anchoring points within PI3Kγ, namely: the peptidic N-Hs of VAL882 and ASP964, albeit the sulfonamide of GDC0941 exhibits an extra interaction with the terminal ammonium of

Table 3
Settings employed in the sequential alignment trials preformed for mTOR kinase domain against the kinase domain of PIK3γ (PDB code: 1E7U).

Trial	Scoring matrix	Gap penalty[a]			Homology model
		Opening	Extending	Separation	
1	Blosum	10	0.05	0.05	A
2	Blosum	100	0.2	0.2	B
3	Gonnet	10	0.05	0.05	–[b]
4	Gonnet	100	0.2	0.2	C
5	Identity	10	0.05	0.05	–[b]
6	Identity	100	0.2	0.2	–[b]
7	Pam	10	0.05	0.05	–[b]
8	Pam	100	0.2	0.2	–[b]

[a] Manually configured ClustalW penalties imposed on gap placements in the alignment procedure.
[b] The resulting ClustalW-based alignments failed in producing corresponding homology models upon submission to SWISS-MODEL.

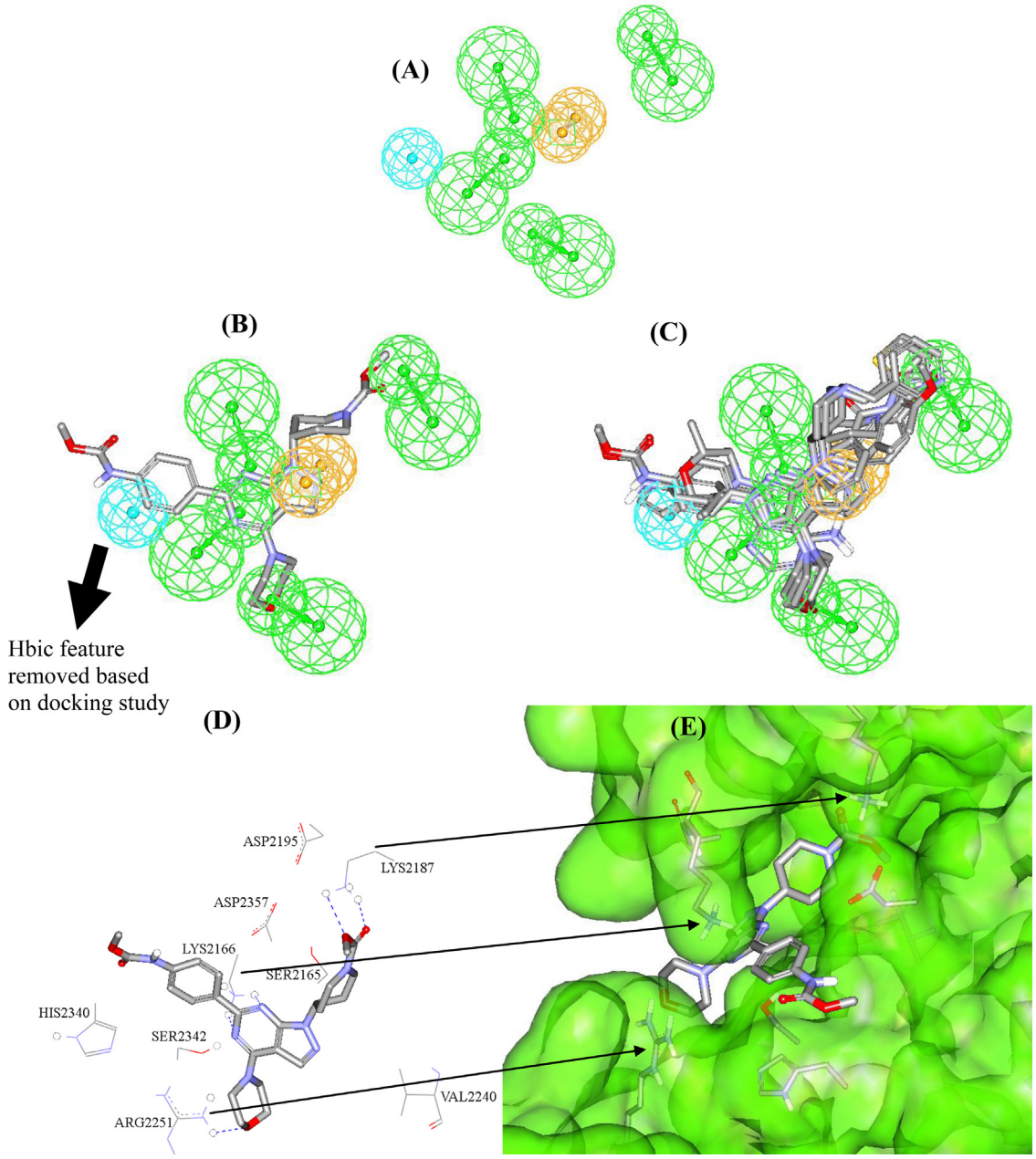

Fig. 3. (A) Hypo1, HBAs are depicted as green vectored spheres, Hbic feature as light blue sphere, and AromRing as vectored orange sphere, (B) Hypo1 fitted against most potent training compound WYE-354 (**5**, IC_{50} = 5 nM), (C) Hypo1 fitted against all training compounds, (D) and (E) Highest-ranking docked pose of **5** (WYE-354) into homology model A of mTOR kinase domain, with and without added Connolly's surface, respectively. Hydrogen bonds are shown as blue dotted lines. (For interpretation of the references to color in this figure legend, the reader is referred to the web version of the article.)

LYS802 [45,46]. On the other hand, the optimal docked pose of **5** has flipped orientation (Fig. 5D), whereby its morpholino fragment is anchored to the guanidinium of ARG2251 at the out rim of mTOR binding pocket, i.e., instead of binding with the peptidic NH of VAL882 (as seen with the analogous morpholine group of GDC0941).

This discrepancy is not unexpected, since the two binding sites of mTOR and PI3Kγ differ in two key binding amino acids, namely: Ser2342 and Arg2251 in mTOR are substituted by Asp950 and Gln893 in PI3Kγ, respectively (Fig. 5A). This difference is expected to cause drastic distinction between the binding modes of ligands within PI3Kγ versus mTOR. Apparently, the morpholino fragment of docked **5** favors strong hydrogen-bonding interactions with the profoundly polarized guanidinium of Arg2251 in mTOR, i.e., preferred over bonding to mildly polarized peptidic N-H of Val882 in PI3Kγ. Moreover, the partially negatively charged heterocyclic nitrogen atoms of pyrazolo-pyrimidine core of **5** seems to favor hydrogen-bonding with Ser2342 in mTOR compared to being repelled by the carboxylate of homologous Asp950 in PI3Kγ.

Furthermore, casting the morpholino moiety above the sterically unhindered Ala2248 at the outer rim of mTOR's binding pocket (Fig. 5A–D) should explain the tolerability of mTOR's binding site to accommodate extra steric substitutions on the morpholine fragments, i.e., compared to PI3Kγ, which exhibits a bulkier Lys890 residue at the same position (Fig. 5A–D). On the other hand, projecting the morpholine ring into the tight binding pouch within the vicinity of Val882 in PI3Kγ probably explains the observed enhancements in mTOR selectivity over PI3Kγ in association with increasing steric bulk of morpholine moieties [45,46].

```
mTOR-210  2161                                                    QVITSKQRP
1E7U      763   VISQLKQKLE NLQNLNLPQS FRVPYDPGLK AGALVIEKC- -KVMASKKKP

mTOR-210  2170  RKLTLMGSN- ----GHEFVF LLKGHEDLRQ DERVMQLFGL VNTLLANDPT
1E7U      811   LWLEFKCADP TALSNETIGI IFKHGDDLRQ DMLILQILRI MESIWETES-

mTOR-210  2215  SLRKNLSIQR YAVIPLSTNS GLIGWVPHCD TLHALIRDYR EKKKILLNIE
1E7U      860   ---LDLCLLP YGCISTGDKI GMIEIVKDAT TIAKIQQSTV GN--------

mTOR-210  2265  HRIMLRMAPD YDHLTLMQKV EVFEHAVNNT AGDDLAKLLW LKSPSSEVWF
1E7U      899   ---------- ---------- ------TGAF KDEVLSHWLK EKCPIEEKFQ

mTOR-210  2315  DRRTNYTRSL AVMSMVGYIL GLGDRHPSNL MLDRLSGKIL HIDFG
1E7U      923   AAVERFVYSC AGYCVATFVL GIGDRHNDNI MIS-ETGNLF HIDFGHINKE
```

Fig. 4. The alignment of mTOR kinase domain and PI3Kγ template (PDB code: 1E7U) that yielded the homology model A. Gaps are shown as (–), identical and similar residues are high-lighted in yellow and green, respectively. Binding site amino acids are indicated with arrow heads. (For interpretation of the references to color in this figure legend, the reader is referred to the web version of the article.)

In conclusion, although our docking places **5** in a pose that disagrees with reported docking poses of mTOR inhibitors *vis-à-vis* the involvement of Val2240 (equivalent to Val882 in PI3Kγ) [45,46], we strongly believe that differences in amino acid composition within the binding pockets of the two homologous proteins should lead to significant differences in the corresponding docked poses.

Further support to the docking experiment comes from close resemblance between interactions unveiled by docking and pharmacophoric features of Hypo1. Clearly from Fig. 3, the pharmacophoric features of Hypo1 closely resemble binding interactions suggested by the docking study: Mapping the central pyrazolopyrimidine system of **5** against two HBA features in Hypo1 (Fig. 3B) corresponds to hydrogen bonding interactions connecting these

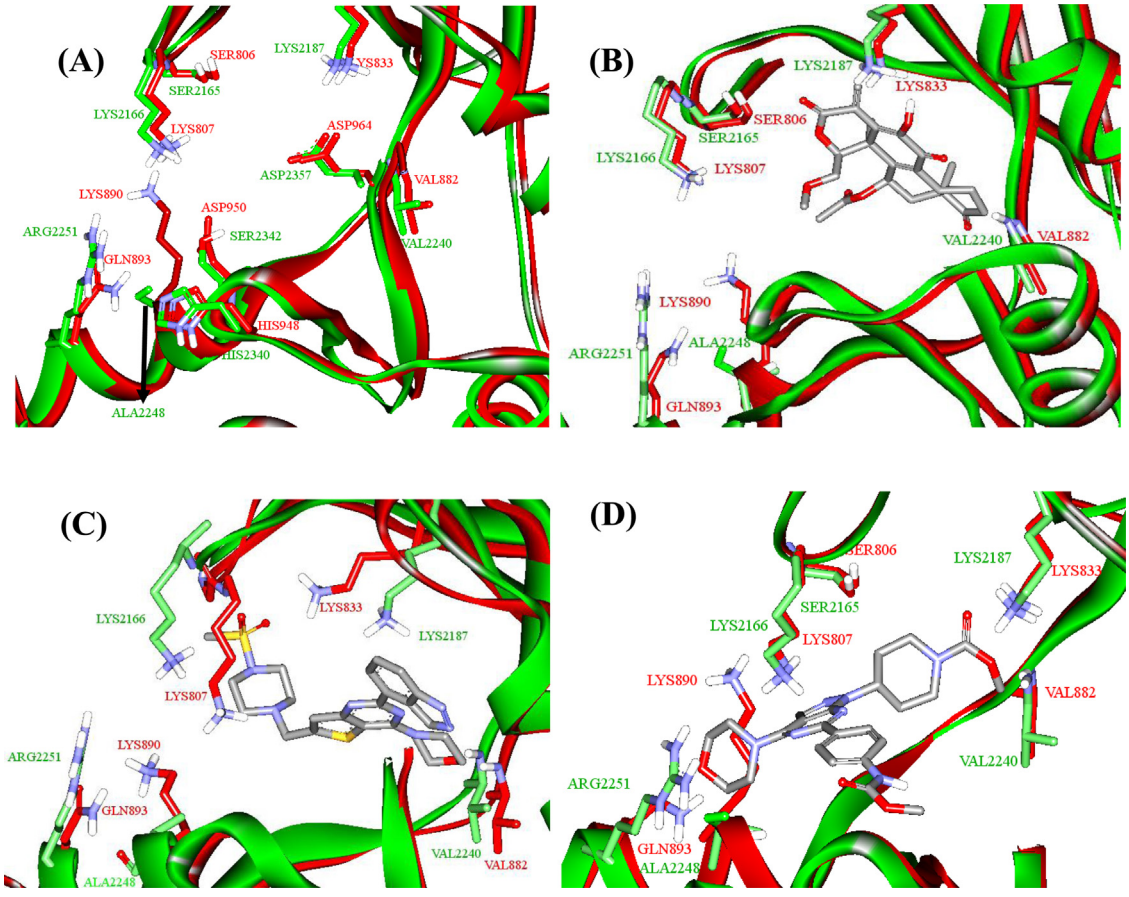

Fig. 5. (A) Detailed view of key amino acids within the binding pocket of mTOR homology model (green) aligned over corresponding amino acids in PI3Kγ template (used to build the homology model, PDB code: 1E7U, red). (B) Binding pocket of mTOR homology model (green) aligned over corresponding amino acids in PI3Kγ (red) co-crystallized with wortmannin (PDB code: 1E7U). (C) Binding pocket of mTOR homology model (green) aligned over corresponding amino acids in PI3Kγ (red) co-crystallized with potent PI3Kγ inhibitor (GDC0941, PDB code: 3DPS). (D) Binding pocket of mTOR homology model (green) including the optimal docked pose of **5** (WYE-354) aligned over corresponding amino acids in PI3Kγ template (1E7U, red). Amino acids labels are colored in red and green corresponding to respective proteins colors.

Table 4
Summary evaluation information produced by the WHAT-CHECK package for the generated homology structures.

Homologue[a]	Packing quality[b]		Ramachandran plot appearance[b]	Chi1/chi2 rotamer normality[b]	Backbone confirmation[b]	Bond[c]		Omega angle restraints[c]	Side chain planarity[c]	Improper dihedral distribution[c]	Inside/outside distribution[c]	Energy (kJ/mol)[d]	Consensus vote[e]
	1st generation	2nd generation				Length	Angles						
A	−1.885	−2.033	−0.964	−1.128	−0.987	0.728	1.107	1.016	1.547	2.242	1.199	−9859	9
B	−2.254	−3.179	−2.725	−2.888	−1.425	0.735	1.148	0.935	1.85	2.253	1.285	−9717	6
C	−2.254	−3.179	−2.725	−2.888	−1.425	0.735	1.148	0.935	1.85	2.253	1.285	−9717	6

[a] Homologue labels as in Table 3.
[b] Positive values are better than average.
[c] Closer to 1.0 is better.
[d] The overall molecular mechanical energy of the model as calculated by SWISS-MODEL.
[e] A consensus voting approach in which each individual WHAT-CHECK property casts a vote if the value of the considered homology structure falls in the highest-ranking 50% of the range of values obtained for that property across the different homology models. The consensus vote is the total number of votes received.

heterocyclic nitrogens with the ε-ammonium group of Lys2166 in the docked model (Fig. 3D and E). Incidentally, previous homology modeling and docking studies seem to ignore the role of Lys2166 in ligand binding/inhibition of mTOR [45,46] which contradicts with the substantial evidence suggesting the significance of central pyrimidine rings (or related analogous heterocycles) for the bioactivities of most mTOR inhibitors, as evident in our pharmacophore training set (compounds **1**–**6** in Fig. 1). In fact, the importance of this core heterocyclic system is clearly evident in Hypo1.

Additionally, mapping the morpholino oxygen and piperidinyl carbamate carbonyl of **5** by two HBA features in Hypo1 agrees nicely with hydrogen bonding interactions tying these groups with the guanidino and terminal ammonium group of Arg2251 and Lys2187, respectively, as in Fig. 3B and D. Finally, mapping the pyrazolo ring of **5** against RingArom feature in Hypo1 seems to correlate with charge-transfer complexation of the electron-deficient pyrazolo ring against the hydroxyl residue of Ser2165.

Interestingly, the hydrophobic feature of Hypo1, which partially maps the benzene ring of **5**, is not represented by any analogous interaction in the docked pose of **5**. In fact, this benzene and its attached methyl carbamate fragment protrude outside the binding pocket as can be seen in Fig. 3E.

In conclusion, homology modeling and docking experiments strongly supported our common feature pharmacophore modeling and subsequent pharmacophore selection based on ROC analyses. Our enhanced confidence in pharmacophore modeling provided impetus to proceed to the subsequent steps of virtual screening and *in vitro* assay.

3.3. In silico screening

Based on our docking study of compound **5**, which suggested the redundancy of the Hbic feature in Hypo1, i.e., being not represented by any corresponding interaction in docking model (see Fig. 3B and E), we decided to delete this feature from Hypo1 to better represent docking-based binding interactions in subsequent virtual screening. Fig. 7A shows the pharmacophoric features of the modified model.

We employed the modified version of Hypo1 (ModHypo1) as 3D-search query against our *in-house*-built database of established drug molecules (1533 compounds). However, we were obliged to allow a maximum of one missed pharmacophoric feature for each captured hit to account for the extremely potent bioactivities of training compounds. Extremely potent training compounds are expected to yield highly limiting binding models, probably unable of capturing moderately potent hits, e.g., known drug molecules.

Virtual screening yielded eight hits captured by ModHypo1. Table 5 shows the captured hits, their fit values and measured anti-mTOR bioactivities, while Fig. 6 shows their corresponding chemical structures.

The mTOR inhibitory activities of captured hits were assessed using Z′-LYTE™ biochemical assay from Invitrogen using PF-04691502 as standard mTOR inhibitor [47] (Fig. 6). Compounds showing % inhibition ≥50% were further analyzed to measure their IC_{50} using GraphPad Prism. The dose–response curves of active hits are depicted in Fig. C in the supplementary materials. Clearly from the figure and Table 5, dose–response curves of captured hits exhibit Hill slope values < 1.0 and excellent correlation coefficients, which strongly suggest the authenticity (i.e., non-promiscuousity) of the inhibitors [60–62].

Interestingly, the β-adrenergic blocker sotalol showed potent anti-mTOR bioactivity with IC_{50} value of 256 nM. Fig. 7B and D compares the docked pose of sotalol with the way it fits ModHypo1. Clearly from the figures, mapping the sulfonamide oxygen atoms of sotalol against the central HBA features in ModHypo1 correlates with hydrogen-bonding interactions tying the

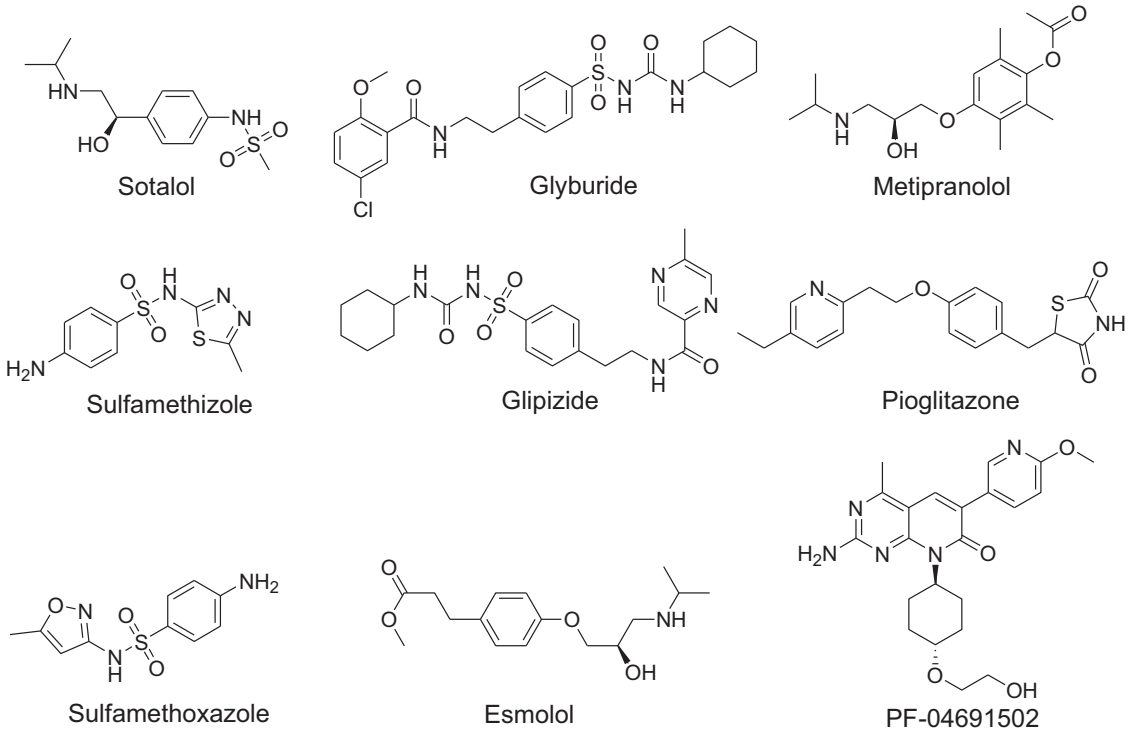

Fig. 6. The structures of captured hits by ModHypo1. PF-04691502 is the standard positive control used in the mTOR inhibitory assay.

sulfonamide with ε-ammonium and guanidine groups of Lys2166 and Arg2251, respectively, in a fashion reminiscent of binding interactions anchoring the central pyrazolo-pyrimidine of training **5** (Fig. 3D). Similarly, mapping the central aromatic ring of sotalol against RingArom feature in ModHypo1 agrees with stacking this ring against the hydroxyl residues of Ser2165 and Ser2342, in a similar sense to the charge transfer complex connecting the pyrazole ring of **5** with the hydroxyl residue of Ser2165. However, fitting the terminal secondary amine of sotalol against HBA feature in ModHypo1 agrees with an electrostatically reinforced hydrogen-bonding interaction connecting this fragment with the carboxylate of Asp2357. A similar interaction is seen with compound **5** albeit with the terminal amino of Lys2187. Nevertheless, the electrostatically reinforced hydrogen-bond with Asp2357 should provide sotalol with equivalent enthalpic binding contributions comparable to hydrogen-bonding interactions tying **5** to Lys2187.

Strangely, we could not find any previous reports linking sotalol with any clinical or pharmacological observation related to its ability to inhibit mTOR bioactivity, which warrants future efforts to investigate the clinical potential of its potent anti-mTOR bioactivity (e.g., its anticancer, anti-Alzheimer's or hypoglycemic potentials).

On the other hand, the oral hypoglycemic sulfonylurea drug, glyburide, which was second best inhibitor in our captured hit list with anti-mTOR IC_{50} of 600 nM, exhibits anticancer, anti-Alzheimer, and

Table 5
The fit values and the inhibitory activities of hits captured by ModHypo1.

Hits[a]	Best fit values against ModHypo1[b]	% of inhibition at 10 μM	IC_{50} (μM)	Hill slope[f]
Sotalol	3.77	89	0.26 ± 0.09[d] (0.99)[e]	0.57
Glyburide	4.13	82	0.6 ± 0.1[d] (0.91)[e]	0.49
Metipranolol	3.47	70	1.3 ± 0.3[d] (0.97)[e]	0.41
Sulfamethizole	3.66	69	1.5 ± 0.4[d] (0.88)[e]	0.56
Glipizide	4.21	54	5.1 ± 1.0[d] (0.95)[e]	0.33
Pioglitazone	3.87	56	5.4 ± 0.9[d] (0.96)[e]	0.49
Esmolol	2.88	41	N.D.	N.D.
Sulfamethoxazole	1.95	28	N.D.	N.D.
PF-04691502[c]	–	100	0.077 ± 0.02[d] (0.98)[e]	0.55

N.D.: not determined.

[a] The compounds and their structures are as in Fig. 6.

[b] After allowing a single missed feature. Fit values against the pharmacophore, calculated as in the following: Fit = $\sum$mapped hypothesis features × W [1 − $\sum$(disp/tol)^2], where $\sum$mapped hypothesis features is the number of pharmacophore features that successfully superimpose corresponding chemical moieties within the fitted compound, *W* is the weight of the corresponding hypothesis feature spheres. This value is fixed to 1.0 in HipHop-generated models. disp is the distance between the center of a particular pharmacophoric sphere and the center of the corresponding superimposed chemical moiety of the fitted compound; tol is the radius of the pharmacophoric feature sphere (known as tolerance, equals 1.6 Å by default). $\sum$(disp/tol)^2 is the summation of (disp/tol)^2 values for all pharmacophoric features that successfully superimpose corresponding chemical functionalities in the fitted compound.

[c] PF-04691502 is the standard positive control applied in mTOR inhibitory assay. The reported IC_{50} of PF-04691502 is 4 nM [47].

[d] This value represent the standard deviation of at least two data points from each concentration.

[e] This value represents the correlation coefficient of the corresponding dose–response line at least three concentrations (0.1, 1, 10 μM and sometimes at 0.01 μM).

[f] Hill slope determined by GraphPad Prism 5.0 [61].

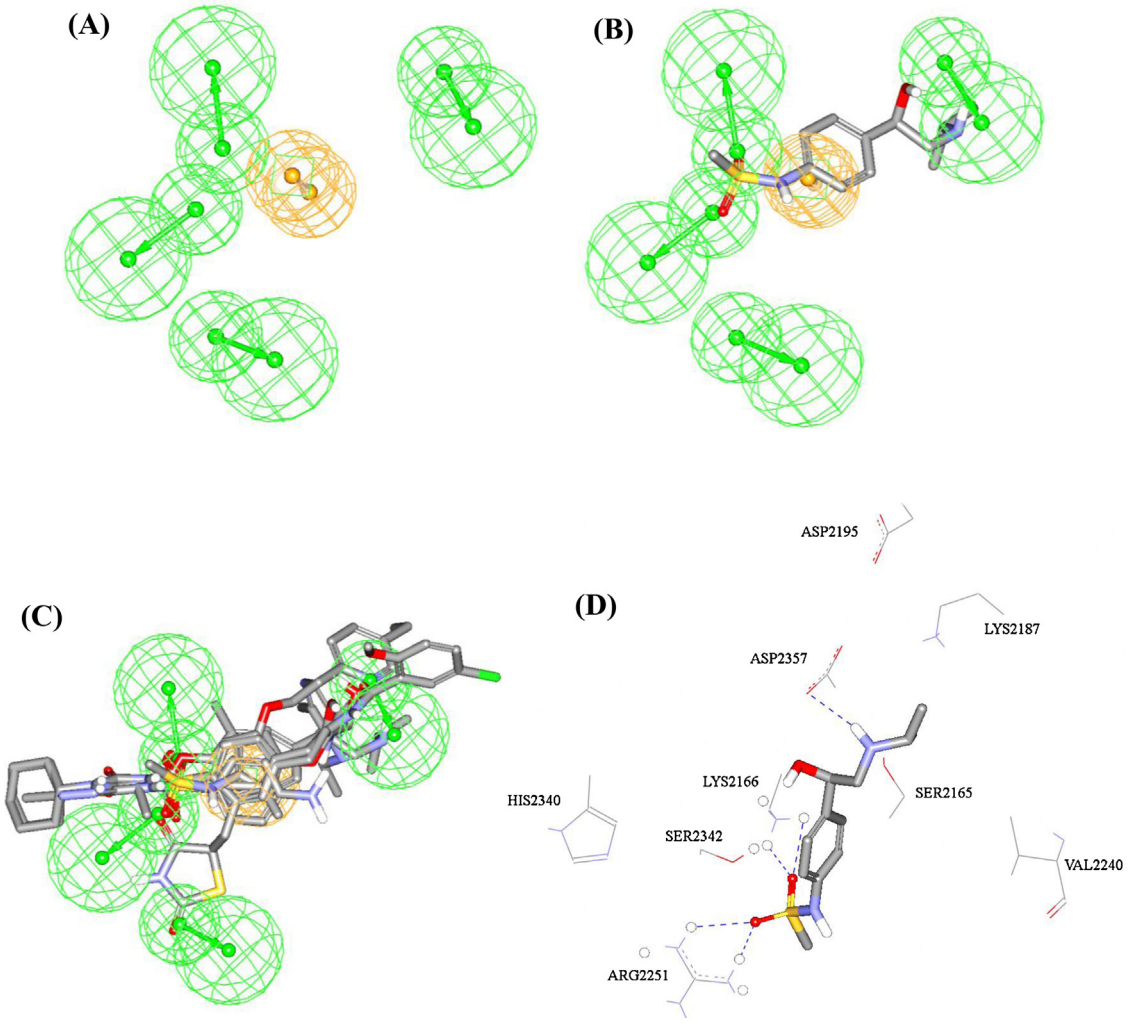

Fig. 7. (A) pharmacophoric features of ModHypo1; ModHypo1 fitted against (B) sotalol (IC_{50} 256.1 nM), (C) all captured hits. HBAs are depicted as green vectored spheres, and AromRing as vectored orange sphere. (D) Top ranking docked pose of sotalol into homology model A of mTOR kinase domain. Hydrogen bonds are shown as blue dotted lines. (For interpretation of the references to color in this figure legend, the reader is referred to the web version of the article.)

hypoglycemic pharmacological properties. Needless to say that these three distinct pharmacological fields are directly related to mTOR inhibition as described in the introduction.

Glyburide have been reported to inhibit progression of many cancers such as bladder carcinoma [48], prostate cancer [49], liver cancer [50], breast cancer [51], and gastric cancer [52]. Furthermore, glyburide arrests breast cancer cells in the G_0/G_1 phase of the cell cycle, resulting in an inhibition of cell proliferation, a mechanism that can also be attributed to mTOR inhibition [8,51]. Moreover; we believe that the ability of glyburide to diminish Aβ toxicity in AD [53] can be partly accredited to mTOR inhibition.

Similarly, the insulin-sensitizer pioglitazon (anti-mTOR IC_{50} = 5.4 μM, Table 5), has established anticancer activities by inhibition cancerous cell proliferation, induction of apoptosis, and arrests cell cycle at G_0/G_1 phase in various cancer diseases; mechanisms not always correlated with peroxisome proliferator activated receptor γ (PPARγ) expression [54–58]. The mTOR inhibitory profile of pioglitazon can be responsible for some of its insulin-sensitizer and anti-aging (longevity) [59] activities.

4. Conclusions

We present a successful example of employing an *in silico* screening, based on robustly designed pharmacophore models in conjunction with ROC analysis and homology modeling of mTOR kinase domain to identify novel compounds with potent mTOR inhibitory activities. With only the very modest effort and expense involved in experimentally screening, we identified five interesting new validated hits having nanomolar to low micromolar affinity. Importantly, the hits identified in our study had wide structural diversity, and little true structural similarity to any of the other known mTOR inhibitors, highlighting an important merit of the virtual screening approach. Because they are established drugs, these hits are expected to be excellent leads for subsequent optimization.

Acknowledgment

The authors thank the Deanship of Scientific Research and Hamdi-Mango Center for Scientific Research at the University of Jordan for their generous funds (Grant No. 108/2011-2012).

Appendix A. Supplementary data

Supplementary data associated with this article can be found, in the online version, at http://dx.doi.org/10.1016/j.jmgm.2013.02.009.

References

[1] D.H. Kim, D.D. Sarbassov, S.M. Ali, J.E. King, R.R. Latek, H. Erdjument-Bromage, P. Tempst, D.M. Sabatini, mTOR interacts with raptor to form a nutrient-sensitive complex that signals to the cell growth machinery, Cell 110 (2002) 163–175.

[2] N. Hay, N. Sonenberg, Upstream and downstream of mTOR, Genes and Development 18 (2004) 1926–1945.

[3] F. Meric-Bernstam, A.M. Gonzalez-Angulo, Targeting the mTOR signaling network for cancer therapy, Journal of Clinical Oncology 27 (2009) 2278–2287.

[4] L.A. Engelman, Targeting PI3K signalling in cancer: opportunities, challenges and limitations, Nature Reviews Cancer 9 (2009) 550–562.

[5] S. Di Paolo, A. Teutonico, D. Leogrande, C. Capobianco, P.F. Schena, Chronic inhibition of mammalian target of rapamycin signaling downregulates insulin receptor substrates 1 and 2 and AKT activation: a crossroad between cancer and diabetes? Journal of the American Society of Nephrology 17 (2006) 2236–2244.

[6] E. Jacinto, R. Loewith, A. Schmidt, S. Lin, M.A. Ruegg, A. Hall, M.N. Hall, Mammalian TOR complex 2 controls the actin cytoskeleton and is rapamycin insensitive, Nature Cell Biology 6 (2004) 1122–1128.

[7] S.C. Land, A.R. Tee, Hypoxia-inducible factor 1alpha is regulated by the mammalian target of rapamycin (mTOR) via an mTOR signaling motif, Journal of Biological Chemistry 282 (2007) 20534–20543.

[8] N. Gao, D.C. Flynn, Z. Zhang, X.S. Zhong, V. Walker, K.J. Liu, X. Shi, B.H. Jiang, G1 cell cycle progression and the expression of G1 cyclins are regulated by PI3K/AKT/mTOR/p70S6K1 signaling in human ovarian cancer cells. American journal of physiology, American Journal of Physiology 287 (2004) C281–C291.

[9] A.S. Don, X.F. Zheng, Recent clinical trials of mTOR-targeted cancer therapies, Reviews on Recent Clinical Trials 6 (2011) 24–35.

[10] T. Chano, H. Okabe, C.M. Hulette, RB1CC1 insufficiency causes neuronal atrophy through mTOR signaling alteration and involved in the pathology of Alzheimer's diseases, Brain Research 1168 (2007) 97–105.

[11] A. Caccamo, S. Majumder, A. Richardson, R. Strong, S. Oddo, Molecular interplay between mammalian target of rapamycin (mTOR), amyloid-beta, and Tau: effects on cognitive impairments, Journal of Biological Chemistry 285 (2010) 13107–13120.

[12] R. Zoncu, A. Efeyan, D.M. Sabatini, mTOR: from growth signal integration to cancer, diabetes and ageing. Nature reviews, Nature Reviews Molecular Cell Biology 12 (2011) 21–35.

[13] K.A. Menear, S. Gomez, K. Malagu, C. Bailey, K. Blackburn, X.L. Cockcroft, S. Ewen, A. Fundo, G.A. Le, G. Hermann, L. Sebastian, M. Sunose, T. Presnot, E. Torode, I. Hickson, N.M. Martin, G.C. Smith, K.G. Pike, Identification and optimisation of novel and selective small molecular weight kinase inhibitors of mTOR, Bioorganic and Medicinal Chemistry Letters 19 (2009) 5898–5901.

[14] K. Tanneeru, L. Guruprasad, Ab initio study of electron transport in 4-(3-nitro-4-tetrafluorophenylthiolate-ethynyl, phenylethynyl) benzenethiolate, Journal of Molecular Modeling 18 (2012) 611–621.

[15] S.B. Bharate, B. Singh, J.B. Bharate, S.K. Jain, S. Meena, R.A. Vishwakarma, QSAR and pharmacophore modeling of N-acetyl-2-aminobenzothiazole class of phosphoinositide-3-kinase-α inhibitors, Medicinal Chemistry Research (2012), http://dx.doi.org/10.1007/s00044-012-0081-3.

[16] H. Li, J. Sutter, R. Hoffmann, HipHop: pharmacophores based on multiple common-feature alignment, in: O.F. Gűner (Ed.), Pharmacophore Perception, Development, and Use in Drug Design, International University Line, California, 2000, pp. 69–84.

[17] A. Smellie, S.L. Teig, P.J. Towbin, Poling – promoting conformational variation, Journal of Computational Chemistry 16 (1995) 171–187.

[18] A. Smellie, S.D. Kahn, S.L. Teig, Analysis of conformational coverage. 2. Application of conformational models, Journal of Chemical Information and Computer Sciences 35 (1995) 295–304.

[19] D. Barnum, J. Greene, A. Smellie, P. Sprague, Identification of common functional configurations among molecules, Journal of Chemical Information and Computer Sciences 36 (1996) 563–571.

[20] HipHop User Guide Version 3.1, Catalyst 4.10, Accelrys Inc., San Diego, CA, 2005. http://www.accelrys.com/doc/life/catalyst410/help/hipHop/HipHop_23TOC.doc.htm

[21] T. Schwede, J. Kopp, N. Guex, M.C. Peitsch, SWISS-MODEL. An automated protein homology-modeling server, Nucleic Acids Research 31 (2003) 3381–3385.

[22] K.S. Wilson, S. Butterworth, Z. Dauter, V.S. Lamzin, M. Walsh, S. Wodak, J. Pontius, J. Richelle, A. Vaguine, C. Sander, R.W. Hooft, G. Vriend, J.M. Thornton, R.A. Laskowski, M.W. MacArthur, E.J. Dodson, G. Murshudov, T.J. Old, R. Kaptein, J.C. Rullmann, Who checks the checkers? Four validation tools applied to eight atomic resolution structures. EU 3-D Validation Network, Journal of Molecular Biology 276 (1998) 417–436.

[23] R. Rodriguez, G. Chinea, N. Lopez, T. Pons, G. Vriend, Homology modeling, model and software evaluation: three related resources, Bioinformatics 14 (1998) 523–528.

[24] J.D. Thompson, D.G. Higgins, T.J. Gibson, CLUSTAL W: improving the sensitivity of progressive multiple sequence alignment through sequence weighting, position-specific gap penalties and weight matrix choice, Nucleic Acids Research 22 (1994) 4673–4680.

[25] S.F. Altschul, W. Gish, W. Miller, E.W. Myers, D.J. Lipman, Basic local alignment search tool, Journal of Molecular Biology 215 (1990) 403–410.

[26] E.H. Walker, M.E. Pacold, O. Perisic, L. Stephens, P.T. Hawkins, M.P. Wymann, R.L. Williams, Structural determinants of phosphoinositide 3-kinase inhibition by wortmannin, LY294002, quercetin, myricetin, and staurosporine, Molecular Cell 6 (2000) 909–919.

[27] C.M. Venkatachalam, X. Jiang, T. Oldfield, M. Waldman, LigandFit: a novel method for the shape-directed rapid docking of ligands to protein active sites, Journal of Molecular Graphics and Modelling 21 (2003) 289–307.

[28] T.W. Sturgill, M.N. Hall, Activating mutations in TOR are in similar structures as oncogenic mutations in PI3KCalpha, ACS Chemical Biology 4 (2009) 999–1015.

[29] A.N. Jain, Scoring non-covalent protein–ligand interactions: a continuous differentiable function tuned to compute binding affinities, Journal of Computer-Aided Molecular Design 10 (1996) 427–440.

[30] A. Krammer, P.D. Kirchhoff, X. Jiang, C.M. Venkatachalam, M. Waldman, LigScore: a novel scoring function for predicting binding affinities, Journal of Molecular Graphics and Modelling 23 (2005) 395–407.

[31] D.K. Gehlhaar, G.M. Verkhivker, P.A. Rejto, C.J. Sherman, D.B. Fogel, L.J. Fogel, S.T. Freer, Molecular recognition of the inhibitor AG-1343 by HIV-1 protease: conformationally flexible docking by evolutionary programming, Chemistry and Biology 2 (1995) 317–324.

[32] D.K. Gehlhaar, D. Bouzida, P. Rejto, Reduced dimensionality in ligand–protein structure prediction: covalent inhibitors of serine proteases and design of site-directed combinatorial libraries, in: L. Parrill, M. Rami Reddy (Eds.), Rational Drug Design: Novel Methodology and Practical Applications, American Chemical Society, Washington, DC, 1999, pp. 292–311.

[33] I. Muegge, Effect of ligand volume correction on PMF scoring, Journal of Computational Chemistry 22 (2001) 418–425.

[34] J.M. Garcia-Martinez, J. Moran, R.G. Clarke, A. Gray, S.C. Cosulich, C.M. Chresta, D.R. Alessi, Ku-0063794 is a specific inhibitor of the mammalian target of rapamycin (mTOR), Biochemical Journal 421 (2009) 29–42.

[35] K. Yu, L. Toral-Barza, C. Shi, W.G. Zhang, J. Lucas, B. Shor, J. Kim, J. Verheijen, K. Curran, D.J. Malwitz, D.C. Cole, J. Ellingboe, S. Ayral-Kaloustian, T.S. Mansour, J.J. Gibbons, R.T. Abraham, P. Nowak, A. Zask, Biochemical, cellular, and in vivo activity of novel ATP-competitive and selective inhibitors of the mammalian target of rapamycin, Cancer Research 69 (2009) 6232–6240.

[36] Z. Zeng, Y.X. Shi, T. Tsao, Y. Qiu, S.M. Kornblau, K.A. Baggerly, W. Liu, K. Jessen, Y. Liu, H. Kantarjian, C. Rommel, D.A. Fruman, M. Andreeff, M. Konopleva, Targeting of mTORC1/2 by the mTOR kinase inhibitor PP242 induces apoptosis in AML cells under conditions mimicking the bone marrow microenvironment, Blood 120 (2012) 2679–3689.

[37] M.E. Feldman, B. Apsel, A. Uotila, R. Loewith, Z.A. Knight, D. Ruggero, K.M. Shokat, Active-site inhibitors of mTOR target rapamycin-resistant outputs of mTORC1 and mTORC2, PLoS Biology 7 (2009) e38.

[38] J. Kirchmair, P. Markt, S. Distinto, G. Wolber, T. Langer, Evaluation of the performance of 3D virtual screening protocols: RMSD comparisons, enrichment assessments, and decoy selection—what can we learn from earlier mistakes? Journal of Computer-Aided Molecular Design 22 (2008) 213–228.

[39] M.L. Verdonk, V. Berdini, M.J. Hartshorn, W.T. Mooij, C.W. Murray, R.D. Taylor, P. Watson, Virtual screening using protein–ligand docking: avoiding artificial enrichment, Journal of Chemical Information and Computer Science 44 (2004) 793–806.

[40] J. Kaplan, J.C. Verheijen, N. Brooijmans, L. Toral-Barza, I. Hollander, K. Yu, A. Zask, Discovery of 3,6-dihydro-2H-pyran as a morpholine replacement in 6-aryl-1H-pyrazolo[3,4-d]pyrimidines and 2-arylthieno[3,2-d]pyrimidines: ATP-competitive inhibitors of the mammalian target of rapamycin (mTOR), Bioorganic and Medicinal Chemistry Letters 20 (2010) 640–643.

[41] A. Zask, J.C. Verheijen, D.J. Richard, J. Kaplan, K. Curran, L. Toral-Barza, J. Lucas, I. Hollander, K. Yu, Discovery of 2-ureidophenyltriazines bearing bridged morpholines as potent and selective ATP-competitive mTOR inhibitors, Bioorganic and Medicinal Chemistry Letters 20 (2010) 2644–2647.

[42] J.C. Verheijen, K. Yu, L. Toral-Barza, I. Hollander, A. Zask, Discovery of 2-arylthieno[3,2-d]pyrimidines containing 8-oxa-3-azabi-cyclo[3.2.1]octane in the 4-position as potent inhibitors of mTOR with selectivity over PI3K, Bioorganic and Medicinal Chemistry Letters 20 (2010) 375–379.

[43] K.J. Curran, J.C. Verheijen, J. Kaplan, D.J. Richard, L. Toral-Barza, L. Hollander, J. Lucas, S. Ayral-Kaloustian, K. Yu, A. Zask, Pyrazolopyrimidines as highly potent and selective, ATP-competitive inhibitors of the mammalian target of rapamycin (mTOR): optimization of the 1-substituent, Bioorganic and Medicinal Chemistry Letters 20 (2010) 1440–1444.

[44] R.W. Hooft, G. Vriend, C. Sander, E.E. Abola, Errors in protein structures, Nature 381 (1996) 272.

[45] A. Zask, J. Kaplan, J.C. Verheijen, D.J. Richard, K. Curran, N. Brooijmans, E.M. Bennett, L. Toral-Barza, I. Hollander, S. Ayral-Kaloustian, K. Yu, Morpholine derivatives greatly enhance the selectivity of mammalian target of rapamycin (mTOR) inhibitors, Journal of Medicinal Chemistry 52 (2009) 7942–7945.

[46] F. Cohen, P. Bergeron, E. Blackwood, K.K. Bowman, H. Chen, A.G. Dipasquale, J.A. Epler, M.F. Koehler, K. Lau, C. Lewis, L. Liu, C.Q. Ly, S. Malek, J. Nonomiya, D.F. Ortwine, Z. Pei, K.D. Robarge, S. Sideris, L. Trinh, T. Truong, J. Wu, X. Zhao, J.P. Lyssikatos, Potent, selective, and orally bioavailable inhibitors of mammalian target of rapamycin (mTOR) kinase based on a quaternary substituted dihydrofuropyrimidine, Journal of Medicinal Chemistry 59 (2011) 3426–3435.

[47] J. Yuan, P.P. Mehta, M.J. Yin, S. Sun, A. Zou, J. Chen, K. Rafidi, Z. Feng, J. Nickel, J. Engebretsen, J. Hallin, A. Blasina, E. Zhang, L. Nguyen, M. Sun, P.K. Vogt, A. McHarg, H. Cheng, J.G. Christensen, J.L. Kan, S. Bagrodia, PF-04691502, a potent and selective oral inhibitor of PI3K and mTOR kinases with antitumor activity, Molecular Cancer Therapeutics 10 (2011) 2189–2199.

[48] R. Wondergem, M. Cregan, L. Strickler, R. Miller, J. Suttles, Membrane potassium channels and human bladder tumor cells: II. Growth properties, Journal of Membrane Biology 161 (1998) 257–262.

[49] M. Abdul, N. Hoosein, Expression and activity of potassium ion channels in human prostate cancer, Cancer Letters 186 (2002) 99–105.

[50] H. Malhi, A.N. Irani, P. Rajvanshi, S.O. Suadicani, D.C. Spray, T.V. McDonald, S. Gupta, KATP channels regulate mitogenically induced proliferation in primary rat hepatocytes and human liver cell lines. Implications for liver growth control and potential therapeutic targeting, Journal of Biological Chemistry 275 (2000) 26050–26057.
[51] K.A. Woodfork, W.F. Wonderlin, V.A. Peterson, J.S. Strobl, Inhibition of ATP-sensitive potassium channels causes reversible cell-cycle arrest of human breast cancer cells in tissue culture, Journal of Cellular Physiology 162 (1995) 163–171.
[52] X. Qian, J. Li, J. Ding, Z. Wang, L. Duan, G. Hu, Glibenclamide exerts an antitumor activity through reactive oxygen species-c-jun NH_2-terminal kinase pathway in human gastric cancer cell line MGC-803, Biochemical Pharmacology 76 (2008) 1705–1715.
[53] X. Chi, E.T. Sutton, G. Hellermann, J.M. Pric, Potassium channel openers prevent beta-amyloid toxicity in bovine vascular endothelial cells, Neuroscience Letters 290 (2000) 9–12.
[54] E. Gottfried, S. Rogenhofer, H. Waibel, L.A. Kunz-Schughart, A. Reichle, M. Wehrstein, A. Peuker, K. Peter, G. Hartmannsgruber, R. Andreesen, M. Kreutz, Pioglitazone modulates tumor cell metabolism and proliferation in multicellular tumor spheroids, Cancer Chemotherapy and Pharmacology 67 (2011) 117–126.
[55] Z. Wan, W. Shi, B. Shao, J. Shi, A. Shen, Y. Ma, J. Chen, Q. Lan, Peroxisome proliferator-activated receptor gamma agonist pioglitazone inhibits beta-catenin-mediated glioma cell growth and invasion, Molecular and Cellular Biochemistry 349 (2011) 1–10.
[56] L. Al-Alem, R.C. Southard, M.W. Kilgore, T.E. Curry, Specific thiazolidinediones inhibit ovarian cancer cell line proliferation and cause cell cycle arrest in a PPARgamma independent manner, PLoS ONE 6 (2011) e16179.
[57] Y. Wang, M. James, W. Wen, Y. Lu, E. Szabo, R.A. Lubet, M. You, Chemopreventive effects of pioglitazone on chemically induced lung carcinogenesis in mice. Molecular cancer therapeutics, Molecular Cancer Therapeutics 9 (2010) 3074–3082.
[58] A. Papi, L. Tatenhorst, D. Terwel, M. Hermes, M.P. Kummer, M. Orlandi, M.T. Heneka, PPARgamma and RXRgamma ligands act synergistically as potent antineoplastic agents in vitro and in vivo glioma models, Journal of Neurochemistry 109 (2009) 1779–1790.
[59] M. Jafari, B. Khodayari, J. Felgner, I.I. Bussel, M.R. Rose, L.D. Mueller, Pioglitazone: an anti-diabetic compound with anti-aging properties, Biogerontology 8 (2007) 639–651.
[60] M.O. Taha, L.A. Dahbiyeh, Y. Bustanji, H. Zalloum, S. Salh, Combining ligand-based pharmacophore modeling, quantitative structure–activity relationship analysis and in silico screening for the discovery of new potent hormone sensitive lipase inhibitors, Journal of Medicinal Chemistry 51 (2008) 6478–6494.
[61] W. Walters, M. Namchuk, Designing screens: how to make your hits a hit, Nature Reviews. Drug Discovery 2 (2003) 259–266.
[62] K.S. Brian, Interpreting steep dose–response curves in early inhibitor discovery, Journal of Medicinal Chemistry 49 (2006) 7274–7277.